Available online at www.sciencedirect.com
ScienceDirect
Science and Technology of Advanced Materials 8 (2007) 357–363
SCIENCE AND TECHNOLOGY OF ADVANCED MATERIALS
www.elsevier.com/locate/stam

Application of spark plasma sintering to the fabrication of binary and ternary skutterudites

C. Recknagel, N. Reinfried, P. Höhn, W. Schnelle, H. Rosner, Yu. Grin, A. Leithe-Jasper*

Max-Planck-Institut für Chemische Physik fester Stoffe, Nöthnitzer Str. 40, 01187 Dresden, Germany

Received 9 May 2007; received in revised form 14 June 2007; accepted 19 June 2007
Available online 30 July 2007

Abstract

Spark plasma sintering (SPS) synthesis of $CoSb_3$ and $LaFe_4Sb_{12}$ from ball-milled elemental metal powders has been performed obtaining samples with high relative densities (~99%). Fracture behaviour, the microstructure and mechanical properties were studied. From ultrasound and nano-indentation measurements, Young's moduli of 148 GPa for $CoSb_3$ and 141 GPa for $LaFe_4Sb_{12}$ were deduced. SPS has been also applied to compact alkali metal and alkaline-earth metal iron antimonides with filled skutterudite structure.

Keywords: Spark plasma sintering (SPS); Skutterudites; $CoSb_3$; $LaFe_4Sb_{12}$; Mechanical properties

1. Introduction

The class of intermetallic compounds known as "skutterudites" exhibits a wealth of topical behaviours, which are the source and motivation of increasing interest and efforts not only to study and understand the underlying physics [1,2], but also to develop them into materials for technological use. All these materials derive from the archetypal mineral skutterudite ($CoAs_3$). Binary semiconducting skutterudites with the formula TX_3 are based on transition metals T = Co, Rh, Ir from the ninth group of the periodic system and the pnictogenes X = P, As and Sb. Ternary skutterudite derivates are based on transition metals from the iron group and need for stabilization of the structural motif electropositive metal cations M leading to the chemical formula MT_4X_{12}.

Here, M usually is a rare-earth or actinide metal which donates electrons to the $[Fe_4Sb_{12}]$ polyanionic host structure [1]. These compounds are called "filled skutterudites" since the stabilizing atoms reside in large voids within the cubic transition metal-pnictogen framework. Recently, a new series of filled skutterudites with monovalent cations Na, K and Tl has been discovered [3,4]. Together with compounds of divalent non-magnetic cations like Ca, Sr, Ba and Yb these skutterudites are well-suited candidates to study the influence of the $[Fe_4Sb_{12}]$ polyanion on physical properties of filled skutterudites [4–6]. From the chemical point of view, the filled skutterudites are iron antimonides of, e.g., alkali metals. The compounds MFe_4Sb_{12} with M = Na, K and Tl exhibit ferromagnetic transitions at $T_C \approx 85$ K with weak itinerant iron magnetic moments and strong spin fluctuations. Moreover they are nearly half-metallic ferromagnets, which are promising materials for spin-electronic devices (spintronics) [4]. A large charge carrier spin polarization up to 67% was found experimentally by point contact spectroscopy [7]. Alkaline-earth metals and Yb-filled skutterudites are paramagnets but several experimental and theoretical observations demonstrate that they are close to ferromagnetic ordering [4,5–8]. In addition, compounds exhibit a pseudogap [9,10] in the infrared optical conductivity which appears at temperatures below 100 K. This phenomenon can be consistently explained by certain sharp peaks in the band structure above E_F [9]. All these iron-based compounds are metals albeit with low metallic conductivity [4].

It is well known that the skutterudites of cobalt-group metals can be doped by void filling only to a certain degree comparing with the iron representatives [1,11]. The filling

*Corresponding author.
E-mail address: jasper@cpfs.mpg.de (A. Leithe-Jasper).

1468-6996/$ - see front matter © 2007 NIMS and Elsevier Ltd. All rights reserved.
doi:10.1016/j.stam.2007.06.007

level can be significantly extended substituting Co by Fe and/or pnictogen by elements of the 4th main group of the periodic table [1,12] leading to the effective increase of polyanion charge.

Currently, interest in semiconducting skutterudite-based materials is mainly fuelled by their possible thermoelectric applications. It turned out that the skutterudites nicely fit into a group of novel thermoelectric materials whose superior properties can be understood within the framework of the ''phonon–glass electron–crystal concept'' [13]. In these materials, a significant depression of the lattice thermal conductivity (thus becoming glass-like with short phonon mean free paths) is due to pronounced scattering of heat-carrying phonons, despite the fact that these compounds are well crystallized with long-range atomic order. This is caused by an intricate interplay between filler atoms and the host structure [13,14]. On the other hand, due to their ordered structure, these materials conduct electricity like a crystal with long electron mean free paths. By this the thermoelectric figure of merit $Z = S^2\sigma/\kappa$ (where S is the thermopower, σ is the electrical conductivity and κ is the thermal conductivity) is enhanced.

A key issue concerning utilization of these intrinsic properties is the experimental and technological accessibility of skutterudite-derived compounds comprising synthesis, processing, machining and testing procedures [15].

Melting and sintering techniques are usual ways to produce skutterudite-based materials. In terms of feasibility the main target is the reduction of heat treatment temperatures and times. Reducing the amount of time and energy-consuming intermediate steps is a rewarding approach. However, laboratory scale conventional melting synthesis of skutterudites involves rather complicated steps, which are hardly suitable for an upscaling and frequently involve the formation of undesired thermodynamically competing phases, target phase decomposition, and problems due to a rather high vapour pressure of the pnictogen constituents at elevated temperatures. For that reason, powder metallurgical approaches utilizing blended metal powders of fine grain size are desirable. Enhancing diffusion together with a shortening of the diffusion paths to ease phase formation and homogenization is therefore preferable. Metallurgical processes which perfectly meet these demands are usually based on a combination of techniques related to mechanical alloying and hot pressing [16–21]. A highly suitable way to fabricate dense skutterudite-based materials is therefore represented by the spark plasma sintering (SPS) technique [22]. The advantages of short sintering time and low sintering temperature due to local discharges generated between the metal particles, thereby activating and purifying their surfaces, make the SPS method the appropriate tool not only for synthesis but also for compaction of skutterudites.

In this work we give a brief overview of the SPS-aided compaction of ternary compounds MFe_4Sb_{12} (M = alkali, alkaline-earth metals). We then address the SPS synthesis and measurement of hardness and elastic moduli of the two compounds $CoSb_3$ and $LaFe_4Sb_{12}$, the former belonging to the family of binary skutterudites, the latter to filled skutterudites based solely on iron as transition metal constituent. $CoSb_3$, being a narrow band gap semiconductor, has been a target of numerous studies concerning routes to its synthesis and tuning of thermoelectric properties [23–26]. $LaFe_4Sb_{12}$ was chosen to study the in situ SPS synthesis of a peritectically forming skutterudite derivative of the air and moisture sensitive rare-earth metal lanthanum. For this purpose a novel SPS system which is integrated into an inert-gas glove-box system has been used [27]. For both compounds the fracture behaviour was also studied.

2. Experimental procedures

2.1. Synthesis

Powders of elements Co, Fe, Sb (99.99 wt%, 325 mesh, Chempur Germany) and La–Sb precursor alloys (200 mesh) at ratios suitable to achieve compositions $CoSb_3$ and $LaFe_4Sb_{12}$ were loaded together with Sialon balls into Sialon grinding vessels (equipped with a gas-tight sealing system) inside an argon glove-box system (partial pressures of O_2 and $H_2O < 0.1$ ppm). Air-sensitive La–Sb alloys were prior synthesized by argon arc melting of La metal (99.9 wt%, RareMetals, China) with appropriate amounts of antimony shot (99.99 wt%, Chempur Germany). Vessels of 45 and 200 ml volume together with balls of 12–15 mm diameter were used. The usual mass ratio of powder to ball was kept at 1:4. Batches of 5–25 g of powders were handled. A planetary ball mill ''Pulverisette 7 classic'' (Fritsch GmbH, Germany) was employed with milling times of about 1 h and rotation speeds of 600–800 rpm. To avoid excessive heating of vessels during milling, the process included equal pauses followed by active periods. After completion the mill charge was removed from vessels inside the glove-box system. No chemical interactions during the milling were obtained according to the X-ray powder diffraction data.

Powder blends were then charged to graphite dies of diameters up to 25 mm which were lined with graphite or tantalum foil and equipped with punch units. Also, graphite dies with rectangular inlays and appropriate punches to fabricate bar-shaped specimens were used. They were then placed in the reaction chamber of an SPS system in a high-purity protection atmosphere designed by cooperative action between SPS Syntex Inc. (Tokyo, Japan), M. Braun GmbH (Garching, Germany), and the MPI CPfS (Dresden, Germany). This system, which is based on a SPS Dr. Sinter 515 machine, is integrated in an argon glove box (partial pressures of O_2 and $H_2O < 0.1$ ppm), thus preventing contamination of reacting powders and reaction products by air and moisture. The SPS machine consists of a uniaxial press combined with a pulsed DC power supply. The pulse regime in this study

was 12 pulses of 3.3 ms each followed by a pause of 6.6 ms. Temperature control during the SPS process was carried out by using a K-type thermocouple located in a hole which was drilled into the graphite die up to 1 mm to the sample/die interface. The actual temperature distribution within the powder sample which depends on the sample material's electrical conductivity and the die wall thickness and material can deviate from the so-measured temperature and thus by this method only an 'apparent' temperature is recorded. Nevertheless, by empirical methods the experimental set-up can be calibrated reasonably well.

The sintered specimens were typically disks of 25 mm in diameter and 3 mm in height or bars of 21 mm length and 5×5 mm front surface. The adhering carbon or tantalum foils could be easily removed.

Alkali and alkaline-earth metal-based iron antimonides were synthesized in multi-step reactions starting from the production of binary low-melting precursor alloys of the highly reactive and air and moisture-sensitive ductile metals with antimony. All these steps were carried out under an atmosphere of inert gas in glove-box systems. Due to the very high vapour pressures of the alkali and alkaline-earth metals these reactions have to be performed in welded metal vessels [4]. $FeSb_2$ can be easily synthesized by SPS and is usually used as the iron containing precursor material. Cold compacted blended powders were then reaction sintered (including several intermediate grinding steps) in welded ampoules at rather low temperatures of 350 °C in case of alkali metal and up to 500 °C for alkaline-earth metal skutterudites, respectively.

Phase analysis was made by powder X-ray diffraction (XRD) using a Guinier Huber G670 imaging plate camera applying Co $K\alpha 1$ radiation ($\lambda = 1.788965$ Å). Lattice parameters were refined using the WinCSD program package [28]. Densities of synthesized specimens were evaluated by the Archimedes method.

Metallographic investigation on polished surfaces was performed with optical microscopy and electron probe microanalysis (EPMA). The latter investigations were done with a wavelength-dispersive (WDX) Cameca SX100 system. Elemental standards for cobalt, iron and antimony and $LaPt_2$ as a lanthanum standard were used. Energy-dispersive analysis (EDX) of the samples was carried out in a Philips XL30 scanning electron microscope.

Images of fracture surfaces were taken with a FEI Quanta 200F ESEM field emission scanning electron microscope.

2.2. Mechanical properties

Vickers hardness was measured at different loads with a MHT-10 microhardness tester mounted on a Carl Zeiss Axioplan 2 optical microscope. Indentations were evaluated using the Olympus analySIS program package.

Elastic moduli were derived from measurements of shear and longitudinal sound velocities, which were measured on disk-shaped samples of $CoSb_3$ and $LaFe_4Sb_{12}$ with a height of 3.4 and 3.07 mm, respectively, at room temperature using a frequency of 5 MHz. In addition, nano-indentation measurements with a Hysitron TriboScope in combination with a Multi-Mode AFM (Digital Instruments) were used to evaluate the elastic moduli.

3. Results and discussion

3.1. SPS compaction of skutterudites at low temperature: alkali metal and alkaline-earth metal-based skutterudites.

The products of conventional powder metallurgical synthesis were usually porous pellets or loose powders. For measurements of physical properties like electrical and thermal transport, specific heat capacity, and optical conductivity, dense samples with well-defined dimensions and surfaces are mandatory. This could be easily achieved by using SPS for compaction. One difficulty which has been encountered here are the rather low temperatures of ≈ 300 °C at which decomposition of alkali metal iron antimonides start. This fact thus necessitated very low process temperatures which were on the other hand detrimental to dense sintering. Nevertheless, the so-compacted samples were there upon accessible to machining and well suited for physical properties measurements [3,4,7–9]. In Fig. 1 the polished surface of a $NaFe_4Sb_{12}$ sample which was SPS treated at 150 °C is shown. No grain growth took place. For SPS-compacted skutterudites MFe_4Sb_{12} (M = Ca, Sr, Ba) similar microstructures were observed.

3.2. SPS synthesis of $CoSb_3$ and $LaFe_4Sb_{12}$

Metallographic and powder XRD analyses revealed that the samples of $CoSb_3$ and $LaFe_4Sb_{12}$ after the first step of spark plasma sintering contain additional phases, namely CoSb, free Co and Sb in the binary sample, and $LaSb_2$,

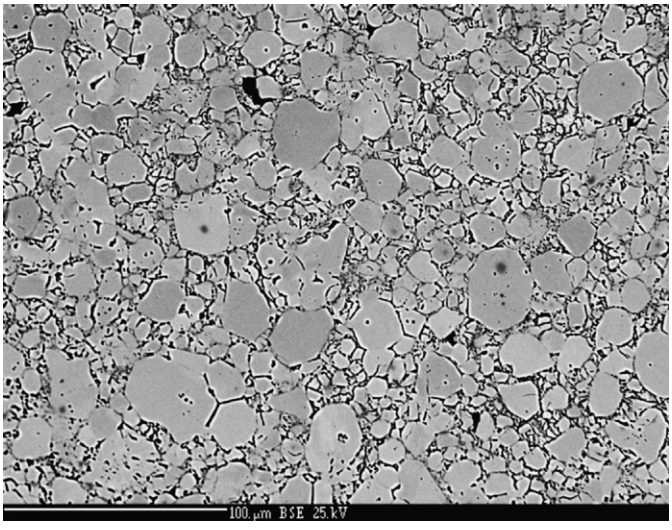

Fig. 1. Micrograph of a SPS-compacted $NaFe_4Sb_{12}$ sample.

Table 1
Optimized SPS parameters for $CoSb_3$ and $LaFe_4Sb_{12}$

Net charge mass (g)	$CoSb_3$		$LaFe_4Sb_{12}$	
	20	3.6	20	3.2
Die diameter, sample dimensions (mm)	25, 5 × 5 × 21	25, 5 × 5 × 21		
Pressure (MPa)	7.3	49.5	20	49.5
Heating rate (°C/min)	20	20	20	20
Holding time (min)	120	30	30	480
Temperature (°C)	550	550	550	600

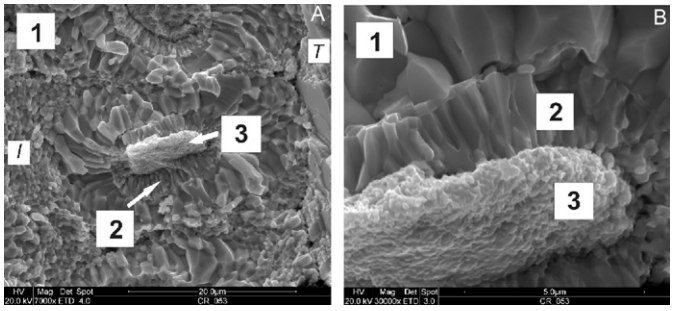

Fig. 2. (A) Fractured surface of a single SPS-sintered $CoSb_3$ specimen. Phase 1: $CoSb_3$ matrix. Phase 2: CoSb. Phase 3: Co nucleation centre. *T*: transgranular fracture, *I*: intergranular fracture. (B) Detail of the CoSb grain boundary with Co nucleus 3, CoSb: 2 and CoSb3 matrix: 3.

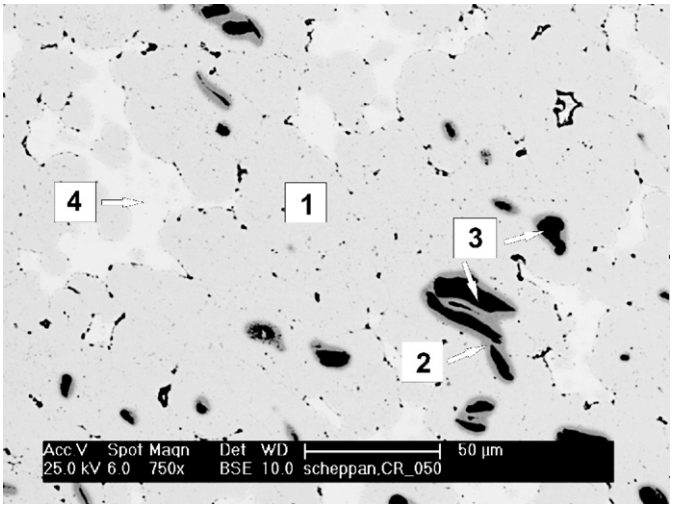

Fig. 3. Back-scattered electron micrograph of a metallographic specimen of $CoSb_3$ after one SPS step. Phase 1: $CoSb_3$. Phase 2: CoSb. Phase 3: Co. Phase 4: Sb.

$FeSb_2$ and Sb in the ternary sample. These findings necessitated regrinding of samples and an additional step of SPS. After these procedures single-phase samples were obtained. The there upon optimized sintering parameters are given in Table 1.

In Fig. 2 we show the fractograph of a $CoSb_3$ specimen after one step of SPS. The bar-shaped sample was subjected to a destructive bending test. It is clearly seen how a Co particle acting as a nucleation centre is surrounded by the CoSb phase followed by the $CoSb_3$ phase enclosing the whole aggregate. Interestingly, no formation of the intermediate $CoSb_2$ phase (which is an equilibrium phase in the Co–Sb binary [29]) takes place, as confirmed by metallographic investigation. In Fig. 3 we can see grains of Co surrounded by CoSb and islands of CoSb in a $CoSb_3$/Sb matrix. Due to their similar material contrast, $CoSb_3$ and Sb are difficult to distinguish in the back scatter electron micrograph. According to the Co–Sb phase diagram $CoSb_3$ forms peritectically from the melt and $CoSb_2$ at 876 °C. CoSb congruently crystallizes from the melt at 1202 °C upon cooling. It seems that at the employed temperatures of 550 °C phase formation of $CoSb_3$ is completed very fast via a two-step reaction of Co with Sb to intermediate CoSb followed by direct conversion to $CoSb_3$. Nevertheless care has to be taken in the evaluation of the applied temperatures in SPS synthesis, since they only represent the temperature of the die. Since we observed no melting and evaporation of volatile antimony ($T_m = 630.8$ °C) during all SPS processes no significant deviations from nominal temperatures in the high limit can be assumed in this study. The whole process is diffusion controlled and depends on the homogeneity of the mixture of reactant powders and their activation. Since compared with the literature data [23,25,26], powder milling times were kept rather short, the beneficial effects of extended mechanical alloying providing a mixture of uniform grain fined and activated particles were obviously not satisfactorily utilized in the present study. This can also be deduced from Fig. 2, where besides the aforementioned formation of the Co–Sb phase a rather heterogeneous distribution of microstructure forming grains can be seen. It has been shown that $CoSb_3$ already forms during long-time high-energy milling of Co and Sb powders [30] which resulted in average grain sizes in nanometer magnitude. Increasing the milling time from 3 to 5 h led to almost single-phase $CoSb_3$. For intermediate milling times, $CoSb_2$ was also observed in multiphase samples. Due to these circumstances, SPS treatment could be reduced to much shorter time scales of a few minutes [24–26]. Nevertheless, formation of a $CoSb_2$ impurity phase in SPS samples only occurs at a rather high temperature of 800 °C and was attributed to Sb volatilization losses which thus change the ratio of reactants [24]. Thus, we can conclude from our study that following the chemical reaction path during the SPS

treatment of mildly milled Co and Sb powders the formation of $CoSb_2$ is inhibited.

Analysing the fracture surfaces we can observe trans- and inter-granular fracture. Here we can assume that the crack formation starts at the non-consumed Co particles. Under load these inclusions then act as regions of high stress in the specimen.

Since the so-fabricated samples showed an inhomogeneous microstructure they were ball-milled again and the powder was then treated by SPS at 550 °C. The fracture surfaces of these specimens look quite different (see Fig. 4). No non-reacted Co grains embedded in the CoSb phase can be detected in the now homogeneous microstructure composed of $CoSb_3$ grains with an average size of about 1 μm. Obviously, no pronounced grain growth takes place at the employed reaction conditions. An intergranular fracture is observed here. No pores are visible, a relative density of 99% could be reached.

Similar observations were made in the case of SPS synthesis of the ternary skutterudite $LaFe_4Sb_{12}$. In Fig. 5 we show the evolution of temperature and densification for the SPS production of single-phase $LaFe_4Sb_{12}$. It can be seen that already after about 25 min and temperatures of 450 °C the reaction sintering is actually completed since no more shrinking of the sample (punch displacement) can be detected. Nevertheless in the experiments the temperature was increased up to 550 °C. In Fig. 6 the fracture surface of a specimen after two SPS treatments with one regrinding step is depicted. A homogeneous intergranular-fractured microstructure is observed with $LaFe_4Sb_{12}$ grains being smaller than 1 μm. The temperature of 600 °C is not high enough to trigger grain growth despite the rather long exposure to SPS. This inhibition of grain growth at temperatures below 700 °C has been also observed in samples of Co-based ternary skutterudites [31]. No pores are visible corresponding well with the rather high observed relative density of 99%.

3.3. Mechanical properties of $CoSb_3$ and $LaFe_4Sb_{12}$

Mechanical properties were measured using SPS specimens which were fabricated as described above. They are

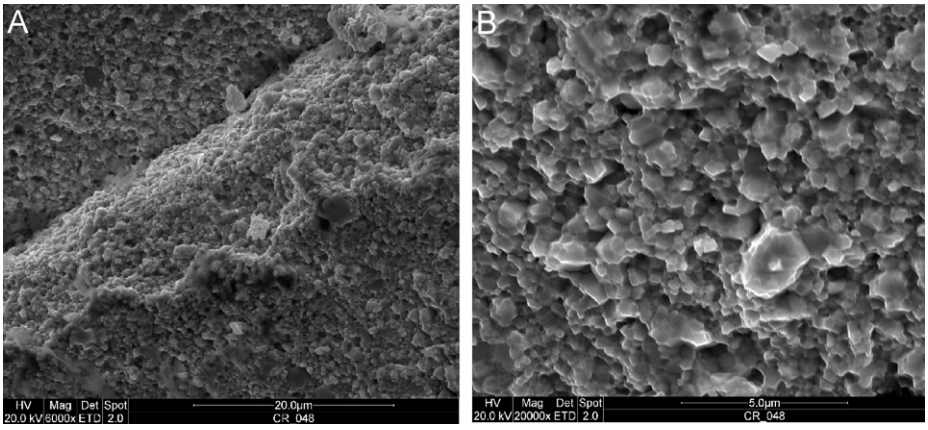

Fig. 4. (A) Fracture surface of single-phase $CoSb_3$ after additional SPS treatment. (B) Details of the microstructure.

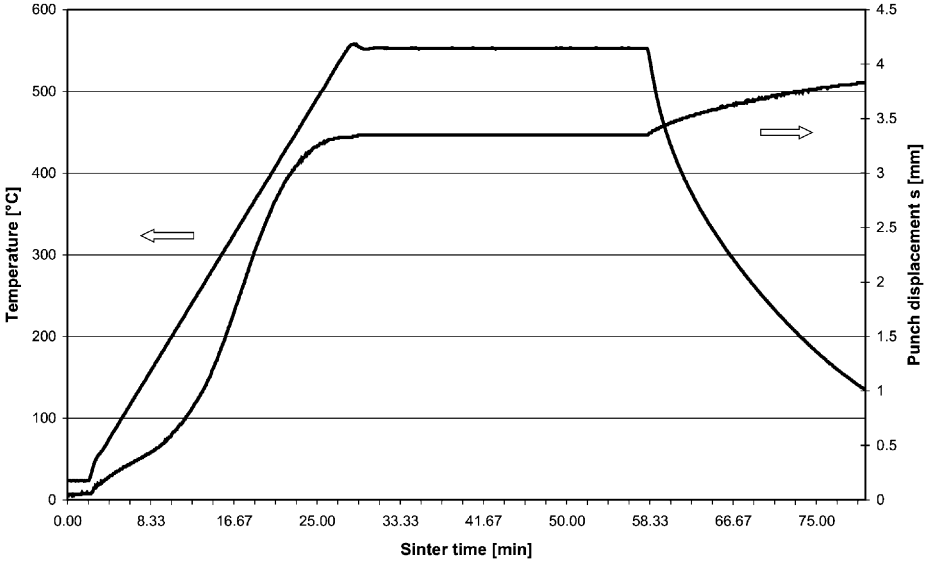

Fig. 5. Evolution of temperature and punch displacement for SPS synthesis of $LaFe_4Sb_{12}$.

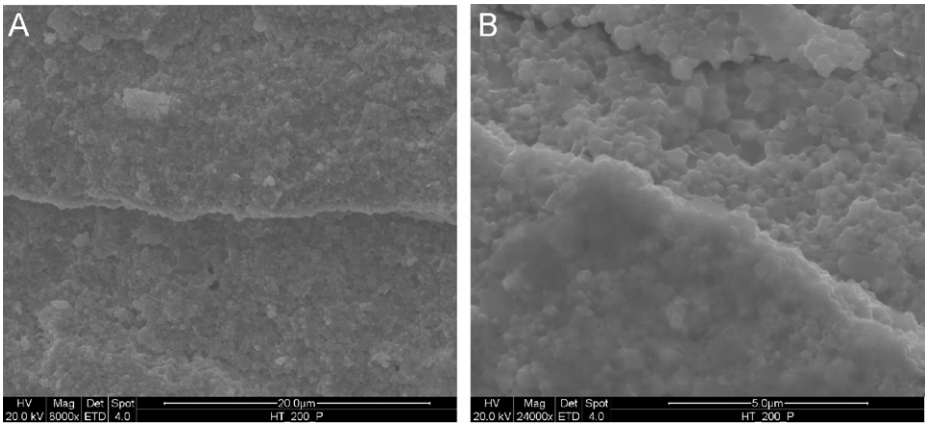

Fig. 6. (A) Fracture surface of single phase SPS-sintered $LaFe_4Sb_{12}$. (B) Details of the microstructure.

Table 2
Crystallographic data and mechanical properties of $CoSb_3$ and $LaFe_4Sb_{12}$

	$CoSb_3$	$LaFe_4Sb_{12}$
Lattice parameter (Å)	9.0353(3)	9.1487(2)
Chemical composition	$Co_{1.01(2)}Sb_{2.99(1)}$	$La_{1.1(1)}Fe_{3.91(5)}Sb_{11.98(5)}$
X-ray density (g/cm^3)	7.62	7.91
Experimental density (g/cm^3)	7.55	7.80
Relative density (%)	99.1	98.7
Vickers hardness HV0.2	608(32)	566(25)
Longitudinal sound velocity (10^5 cm/s)	4.76	4.60
Shear sound velocity (10^5 cm/s)	2.833	2.708
Young's modulus E (GPa)	148(26)	141(20)
Bulk modulus K (GPa)[a]	89.9	88.7

[a] $K = E/3(1-2v)$ with the Poisson ratio v.

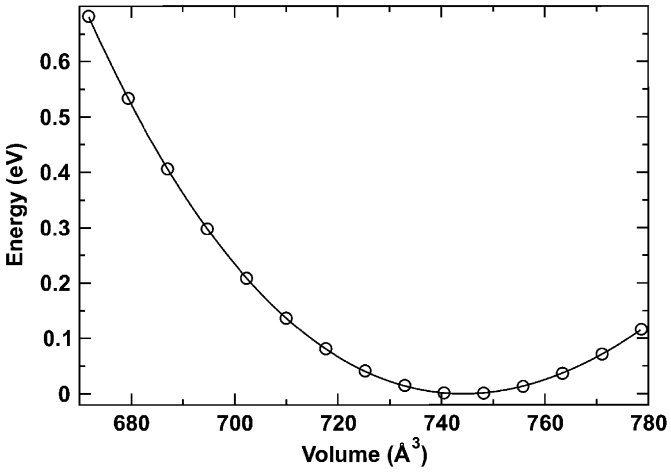

Fig. 7. Calculated total energy of $LaFe_4Sb_{12}$ vs. unit cell volume.

listed together with the refined lattice parameters in Table 2. To check for possible density inhomogeneities, microhardness was mapped on several cross sections of the specimens. A homogeneous distribution of HV 0.2 values was observed in case of both compounds with no significant differences between different regions of the samples' margins and interior areas thus emphasizing the suitability of the SPS method for producing dense samples with an uniform microstructure.

From the measured longitudinal (v_l), shear (v_s) sound velocities and density (ρ) Young's modulus E can be calculated (see Table 2):

$$E = \rho \frac{3v_s^2 v_l^2 - 4v_s^4}{v_l^2 - v_s^2}.$$

For $CoSb_3$ measured sound velocities are in good agreement with the literature data which were measured on single crystals ($v_l = 4.590 \times 10^5$ and $v_s = 2.643 \times 10^5$ cm/s) [32]. For both compounds the Young's moduli deduced from ultrasound measurements of 148(26) GPa for $CoSb_3$ and 141(20) GPa for $LaFe_4Sb_{12}$, respectively, are similar within error margins (see Table 2). With the nano-indentation method a Young's modulus of 148 GPa was also found for $CoSb_3$. For $LaFe_4Sb_{12}$ the derived modulus of 130 GPa is slightly smaller compared to the value extracted from the sound measurement but comparable within the error margins (20 GPa).

It is now interesting to compare experimental values with values derived from electronic band structure LDA calculations where the total energy as function of volume can be fitted to the Birch–Murnaghan equation of state (see Fig. 7). A theoretical lattice parameter of 9.06 Å and bulk modulus of 101.4 GPa were found for $LaFe_4Sb_{12}$. Compared with the experimentally derived lattice parameter of 9.1487(2) Å the calculated one is slightly smaller. Keeping in mind that due to this well-known underestimation of bond lengths in the Local Density Approximation (LDA) the calculated bulk modulus usually exceeds the measured bulk modulus by about 10–20%, a good agreement with the experimentally observed 88.7 GPa is found. Similarly, for $CoSb_3$ Feldman et al. [33] calculated a bulk modulus of 105 GPa compared with 89.9 GPa derived from our sound measurements. Thus, for both compounds the same trends

between theoretical and experimental values are observed with the lattice of $CoSb_3$ being slightly stiffer than that of $LaFe_4Sb_{12}$.

4. Conclusions

Spark plasma sintering were used to compact alkali metal and alkaline-earth metal-based iron antimonides at rather low temperatures. Applying the SPS process, highly densified samples of skutterudites $CoSb_3$ and $LaFe_4Sb_{12}$ could be prepared and their mechanical properties were measured. After an intermediate milling and additional SPS step they have a homogeneous microstructure. Destructive bending results in intergranular fracture. $CoSb_3$ forms in a non-equilibrium two-step reaction from Co and Sb powders via the intermediate phase CoSb. No formation of $CoSb_2$ is observed. Elastic moduli of 148(26) and 141(20) GPa were deduced from sound velocity measurements for $CoSb_3$ and $LaFe_4Sb_{12}$, respectively. They can be substantiated by additional nano-indentation measurements. The theoretically deduced values for the bulk moduli are in good agreement with the experimentally measured ones exceeding them by about 10%.

Acknowledgements

The authors are indebted to G. Auffermann, U. Burkhardt, P. Scheppan, H. Tlatlik, P. Simon for chemical analysis, help with metallographic characterization, surface visualization and EPMA. The help of R. Cardoso-Gil with powder XRD is acknowledged. The authors especially appreciate the support of Prof. B. Kieback and Prof. M. Schaper at the Institut für Werkstoffwissenschaften, Technische Universität Dresden who made the use of testing units at the laboratory for mechanical materials testing available to us. G. Garg at TU Dresden is acknowledged for performing the nano-indentation experiments. The Emmy–Noether–Programme of the Deutsche Forschungsgemeinschaft is acknowledged for financial support (H.R.). The authors also like to thank the reviewers for instructive comments.

References

[1] C. Uher, Semiconduct Semimet 68 (2001) 139.
[2] B.C. Sales, in: K.A. Gschneidner Jr., J.C.G. Bünzli, V.K. Pecharsky (Eds.), Handbook on the Physics and Chemistry of Rare Earths, vol. 33, Elsevier, Amsterdam, 2003, p. 1 Chapter 211.
[3] A. Leithe-Jasper, W. Schnelle, H. Rosner, N. Senthilkumaran, A. Rabis, M. Baenitz, A.A. Gippius, E.N. Morozova, J.A. Mydosh, Yu. Grin, Phys. Rev. Lett. 91 (2003) 037208.
[4] A. Leithe-Jasper, W. Schnelle, H. Rosner, M. Baenitz, A. Rabis, A.A. Gippius, E.N. Morozova, H. Borrmann, U. Burkhardt, R. Ramlau, U. Schwarz, J.A. Mydosh, Yu. Grin, Phys. Rev. B 70 (2004) 214418.
[5] T. Takabatake, E. Matsuoka, S. Narazu, K. Hayashi, S. Marimoto, T. Sasakawa, K. Umeo, M. Sera, Physica B 383 (1) (2006) 93–102.
[6] E. Matsuoka, K. Hayashi, A. Ikeda, K. Tanaka, T. Takabatake, M. Matsumura, J. Phys. Soc. Jpn 74 (5) (2005) 1382–1385.
[7] G. Sheet, H. Rosner, S. Wirth, A. Leithe-Jasper, W. Schnelle, U. Burkhardt, J.A. Mydosh, P. Raychaudhuri, Yu. Grin, Phys. Rev. B 72 (2005) 180407.
[8] W. Schnelle, A. Leithe-Jasper, M. Schmidt, H. Rosner, H. Borrmann, U. Burkhardt, J.A. Mydosh, Yu. Grin, Phys. Rev. B 72 (2005) 020402(R).
[9] J. Sichelschmidt, V. Voevodin, H. Im, S. Kimura, H. Rosner, A. Leithe-Jasper, W. Schnelle, U. Burkhardt, J.A. Mydosh, Yu. Grin, Phys. Rev. Lett. 96 (2006) 037406.
[10] S. Kimura, T. Mizuno, H. Im, K. Hayashi, E. Matsuoka, T. Takabatake, Phys. Rev. B 73 (2006) 214416.
[11] X. Shi, W. Zhang, L.D. Chen, J. Yang, Phys. Rev. Lett. 95 (2005) 185503.
[12] B.C. Sales, D. Mandrus, B.C. Chakoumakos, V. Keppens, J.R. Thomson, Phys. Rev. B 56 (1997) 15081–15089.
[13] G.A. Slack, CRC Handbook of Thermoelectrics, in: D.M. Rowe (Ed.), Chemical Rubber, Vol. 33, CRC Press, Boca Raton, FL, 1995, p. 407 (Chapter 34).
[14] G.S. Nolas, G.A. Slack, D.T. Morelli, T.M. Tritt, A.C. Ehrlich, J. Appl. Phys. 79 (1996) 4002–4008.
[15] H.H. Saber, M.S. El-Genk, T. Caillat, J. Energy Conv. Manage. 48 (2007) 555–567.
[16] S. Bao, J. Yang, W. Zhu, X. Fan, X. Duan, J. Peng, Mater. Lett. 60 (2006) 2029–2032.
[17] S.Q. Bao, J.Y. Yang, X.L. Song, J.Y. Peng, W. Zhu, X.A. Fan, X.K. Duan, Mater. Sci. Eng. A 438–440 (2006) 186–189.
[18] S. Bao, J. Yang, J. Peng, W. Zhu, X. Fan, X. Song, J. Alloys Compd. 421 (2006) 105–108.
[19] X. Song, J. Yang, J. Peng, Y. Chen, W. Zhu, T. Zhang, J. Alloys Compd. 399 (2005) 276–279.
[20] J. Yang, Y. Chen, W. Zhu, J. Peng, S. Bao, X. Fan, X. Duan, J. Solid State Chem. 179 (2006) 212–216.
[21] S. Bao, J. Yang, W. Zhu, X. Fan, X. Duan, J. Peng, Mater. Lett. 60 (2006) 2029–2032.
[22] M. Tokita, J. Soc. Powder Tech. Jpn. 30 (1993) 790–804.
[23] W.S. Liu, B.P. Zhang, J.F. Li, L.D. Zhao, J. Phys. D 40 (2007) 566–572.
[24] K. Liu, D. Xiang, J. Zhang, Rare Metals 24 (3) (2005) 257–260.
[25] J.X. Zhang, Q.M. Lu, K.G. Liu, L. Zhang, M.L. Zhou, Mater. Lett. 58 (2004) 1981–1984.
[26] R. Hara, S. Inoue, H.T. Kaibe, S. Sano, J. Alloys Compd. 349 (2003) 297–301.
[27] N. Reinfried, P. Höhn, Yu. Grin, Scientific Report MPI CPfS (2006) 28–31.
[28] L.G. Akselrud, P.Y. Zavalii, Y.u. Grin, V.K. Pecharsky, B. Baumgartner, E. Wölfel, Mater. Sci. Forum 133–136 (1993) 335.
[29] T.B. Massalski (Ed.), Binary Alloy Phase Diagrams, vol. 2, ASM International, Materials Park, Ohio, 1990, pp. 1232–1234.
[30] K. Liu, J.X. Zhang, D. Xiang, J. Mater. Process. Tech. 184 (2007) 257–260.
[31] L. Yang, J.S. Wu, L.T. Zhang, Mater. Design 25 (2004) 97–102.
[32] T. Caillat, A. Borshchevsky, J.-P. Fleurial, J. Appl. Phys. 80 (8) (1996) 4442–4449.
[33] J.L. Feldman, D.J. Singh, Phys. Rev. B 53 (1996) 6273–6282.